Cement and Concrete Research 113 (2018) 86–98

Contents lists available at ScienceDirect

Cement and Concrete Research

journal homepage: www.elsevier.com/locate/cemconres

Water penetration through cracks in self-healing cementitious materials with superabsorbent polymers studied by neutron radiography

D. Snoeck*, P. Van den Heede, T. Van Mullem, N. De Belie

Magnel Laboratory for Concrete Research, Department of Structural Engineering, Faculty of Engineering and Architecture, Ghent University, Tech Lane Ghent Science Park, Campus A, Technologiepark Zwijnaarde 904, B-9052 Gent, Belgium

ARTICLE INFO

Keywords:
Microcracking
Absorption
Permeability
Polymers
Fiber reinforcement

ABSTRACT

SuperAbsorbent Polymers (SAPs) are a promising admixture to obtain self-sealing and self-healing cementitious materials. They are able to physically block water penetration through cracks due to their swelling ability. This is very useful in a cementitious material which is prone to cracking leading to a reduced durability. The effectiveness of counteracting water penetration is of concern. Neutron radiography was performed in order to investigate the influence of SAPs on the water permeability through healed cracks with respect to a reference material without SAPs. The gravimetrically measured capillary absorption corresponded with the obtained results after image analysis and a quantitative analysis could be made. SAPs enhance the water impermeability and are able to seal and heal a crack effectively up to 100 μm. The healing was a main factor to impede water movement through cracks. This will lead to less water ingress in building infrastructures and a possible longer service life.

1. Introduction

Cracking in concrete and especially the possible eventual gas or water ingress through these cracks is a major concern for buildings and infrastructures. The water may contain harmful substances which can start to deteriorate the cementitious material and may also lead to corrosion of the reinforcement. As effective manual crack repair may be difficult due to inaccessibility, a self-healing material can be used. This material is able to self-repair occurring cracks without the need for external repair and human intervention. Different approaches are possible, ranging from the use of encapsulated polymers [1–4], over calcium carbonate precipitating bacteria [5–8] and microcapsules [9–11], crystalline admixtures [12–14] and vascular systems [15–17], to synthetic microfibres [18–21] and SuperAbsorbent Polymers (SAPs) [22–24].

The SAPs are a new promising admixture for cementitious materials [25]. They are able to absorb up to thousand times their own weight in liquid [26]. They can be used for internal curing [27–30], to increase the freeze-thaw resistance [31, 32], to change the rheology [33], as well as to induce self-sealing [34–36] and self-healing [22–24] of cementitious materials. Their self-sealing and self-healing ability is interesting in terms of the permeability of a cementitious material. As the superabsorbent polymers swell, they will physically block a crack from intruding fluids. This will lead to a regain in impermeability of the cementitious material. In that way, less harmful substances will intrude the material and the durability is less endangered. This self-sealing effect occurs instantaneously. It will depend on the swelling time of the SAP which is in the order of several seconds to tens of seconds. The amount and size of the added SAPs needs to ensure proper sealing. An amount of 1 m% and an average size of 500 μm seems to be efficient [36, 37]. Furthermore, the absorbed water can be used to stimulate and promote autogenous healing. Autogenous healing, in the form of further hydration of cement, pozzolanic activity of supplementary cementitious materials and calcium carbonate crystallization, can visually close cracks [22, 24]. Complete healing is possible up to 30–50 μm crack widths in strain-hardening cementitious composites [18, 24]. This healing leads thus to a physical pertinent closure of the cracks. In that way, harmful gases may also no longer penetrate the structure and the mechanical properties are regained [22, 24].

Depending on the efficiency of the (promoted) healing, the cracks may show less or no water penetration over time. This can be studied by means of capillary water absorption or water permeability tests, but the water distribution can not to be studied in detail. It has not been studied whether the crack healing action provides full sealing or healing of the crack or whether there is still a part of the crack where water may penetrate. Therefore, in this paper, the capillary water absorption results are linked to neutron radiography analyses which can clearly visualize water in a cementitious material as a function of time. In that

* Corresponding author.
E-mail addresses: nele.debelie@UGent.be (D. Snoeck), didier.snoeck@UGent.be (N. De Belie).

https://doi.org/10.1016/j.cemconres.2018.07.002
Received 8 November 2017; Received in revised form 4 May 2018; Accepted 12 July 2018
Available online 27 July 2018
0008-8846/

way, the (im)permeability can be studied in great detail and conclusions can be drawn on the effectiveness of the sealing and healing of cracks in cementitious materials with and without SAPs.

Neutron radiography is a powerful technique to non-destructively study fluids containing hydrogen in a system. It has been applied on cementitious materials to study the water movement through cracks as the technique can be used to visualize and quantitatively evaluate the kinetics of water ingress into porous solids [38–40]. A study on concrete strengthened by strain-hardening cementitious materials showed that neutron radiography is able to prove the effectiveness of a repair product [41]. Also water repellents which hydrophobize cracks preventing water movement were studied [42, 43]. Furthermore, the water release of the SAPs can be studied by neutron radiography measurements during hydration of the cementitious material [44]. The SAP particle shrinks as it releases its stored mixing water and an empty macro pore remains [45], possibly partly filled with hydration products [46]. Autogenous healing by SAPs was not studied up till now with neutron imaging. The water penetration through cracks autonomously healed by encapsulated polyurethane-based agents, was studied and it was found that the ingress of water into the crack can be prevented depending on the type of agent [40]. However, in presence of two or more cracks, only one can be properly healed by this approach [47]. The current study continues on the previously mentioned research since neutron radiography results regarding the water permeability through autogenously healed cementitious materials with and without SAPs are lacking in literature.

2. Materials and methods

In this section, the two different studied mixtures and samples are described (Section 2.1). Next, the cracking method (four-point-bending) and the microscopic analysis are discussed (Section 2.2). The capillary absorption measurements are explained next (Section 2.3). In the end, the neutron radiography principle and apparatus together with the performed image analysis to investigate the water movement through the cracked material is explained (Section 2.4).

2.1. Studied mixture compositions

Two mortar mixes (REF and SAP) were studied in detail and consisted out of cement (CEM I 52.5 N, Holcim, Belgium), fly ash (Class F, OBBC, Belgium), fine silica sand (M34, D_{50} = 170 μm, Sibelco, Belgium), a polycarboxylate-type superplasticizer (Glenium 51 conc. 35%, BASF, Belgium), PVA microfibres (oil-coated, 15 dtex, 8 mm cutting length, 12 cN/dtex, Kuraray, Japan), water and, depending on the mixture, superabsorbent polymers. The chemical composition of the cement and fly ash can be found in [22, 30].

The SAP used is called SAP B, a cross-linked potassium salt polyacrylate (particle size 476.6 ± 52.9 μm (n = 100)). The nomenclature of the SAP is the same as in previous research of the authors [22–24, 36]. The SAP is bulk-polymerized and consists of irregular crushed particles. It is able to absorb 283.2 ± 2.4 g/g SAP in demineralized water and 58.4 ± 1.7 g/g SAP in cement filtrate solution. The swelling time in a fluid to full absorption was 60 ± 5 s in standard laboratory conditions (a temperature of 20 ± 2 °C and a RH of 60 ± 5%). The absorption capacity was determined using the filtration method and the swelling time using the vortex method [26].

The mortar composition can be found in Table 1 and is based on the research of Li et al. [18, 48] and Snoeck et al. [22, 24]. The fly ash-to-cement ratio was 1, the sand-to-binder ratio was 0.35, the superplasticizer-to-binder ratio amounted to 0.005 and the water-to-binder ratio was 0.3 for both mixtures. An amount of 2 v% of PVA fibres was added to ensure strain-hardening. The SAP-to-cement ratio was 0.01 (1 m% of cement weight). Additional water was added to the SAP mixture to ensure no loss in workability. This amount is the ideal amount which is absorbed and was verified using optical microscopy [49, 50] and X-ray computed microtomography [23]. The effective water-to-binder ratio is the same for the REF and the SAP mixture.

The SAP was stored in dry and sealed conditions prior to testing or mixing in the cement paste mixture. First, the cement, fly ash and possibly SAPs (depending on the mixture composition) were equally distributed with a mortar mixer. Then, the total amount of water and superplasticizer were added and mixed for 30 s at 140 rpm. The fine silica sand was added during the next 30 s at 140 rpm. To ensure a homogeneous dispersion of all components, the speed was increased for the following 30 s to 285 rpm. The edges of the bowl were scraped during 30 s and the mixture was then allowed to rest for a period of 60 s. Subsequently, while mixing at a speed of 140 rpm, microfibres were slowly added during 30 s. The final step was mixing for 60 s at 285 rpm.

Moulds (160 × 20 × 40 mm^3) which had a rebar (sandpapered messing surface with 2 mm diameter) at a height of one third of the total height were filled and the samples were compacted by jolting 60 times. The moulds were then covered using plastic foil and put at a temperature of 20 ± 2 °C. The samples were demoulded after 48 h and were stored wrapped in plastic foil at a temperature of 20 ± 2 °C until the age of 28 days. Series used within this study consisted of minimum three 160 × 20 × 40 mm^3 samples per healing condition and per test method in order to obtain statistical sound results.

2.2. Cracking and healing conditions with microscopic analysis

After being stored for 28 days, the specimens were cracked using a four-point-bending test. The bottom side of the specimens is equal to 160 × 20 mm^2. A servo hydraulic testing system (Walter + Bai DB 250/15) ensured a displacement-controlled test (0.005 mm/s to imitate a quasi-static load). The lower and upper supports were 140 mm and 50 mm apart from each other, respectively. The strain at the bottom side of the specimen was limited to 2.5%, theoretically calculated from the curvature and the vertical displacement during loading. This strain is lower than, but close to, the maximum possible strain at ultimate strength (3–4% [37]) of such a strain-hardening specimen, so the actual service cracks could be studied.

After four-point-bending, the cracks were measured using an optical microscope (Leica S8 APO mounted with a DFC 295 camera). Then, the specimens were stored in three different conditions for 28 days to allow crack healing:

1) At 20 ± 2 °C with application of wet/dry cycles (alternatively stored in demineralized water for 1 h, and exposed to a relative humidity (RH) of 60 ± 5% for 23 h);
2) In a room with a RH = 95 ± 5% (> 90%);
3) In a room with a RH = 60 ± 5%.

REF samples were exposed to the first two healing conditions and SAP samples to all three healing conditions. Storing REF samples in a

Table 1
Mortar composition of the studied mixtures.

Sample code	Cement [kg/m^3]	Fly ash [kg/m^3]	Sand [kg/m^3]	Water [kg/m^3]	Superplasticizer [kg/m^3]	PVA Fibres [kg/m^3]	SAP [kg/m^3]
REF	611	611	428	367	6	26	0
SAP	575	575	402	396	6	26	5.75

RH condition of 60% would result in approximately the same healing as at a RH of > 90%, i.e. almost none [23]. To use the measuring time as efficiently as possible, these specimens were thus not studied as no additional information would be obtained.

After 28 days healing, the cracks were once more studied microscopically. The visual closure of the crack width served as a qualitative measure for the autogenous healing capacity. The percentage is calculated as the difference between the subsequent measurements and the initial crack width immediately after cracking and unloading of the specimens.

Additionally, the compressive strength was measured (NBN EN 196-1) on 160 × 40 × 40 mm^3 mortar beams with a testing machine Walter + Bai DB 250/15. The mechanical properties were studied at 28 days after casting. The samples were stored at a relative humidity of > 95% and a temperature of 20 ± 2 °C until the age of testing.

2.3. Capillary water absorption tests

Three 160 × 20 × 40 mm^3 specimens per test series and healing condition were subjected to capillary water absorption tests in analogy with the standard EN 13057. At the age of 56 days, all samples were first dried in an oven at 50 ± 1 °C for 7 days to exclude all moisture, prior to testing. All surfaces, except the bottom and top faces of the specimens, were covered with self-adhesive aluminium foil to induce unidirectional water flow during the test. The lower surface contained the multiple (un)healed crack mouths through which the water may penetrate. The samples were put on supports and immersed for 3 mm in water. The method uses the increase in weight (0.01 g accuracy) due to capillary absorption of water over a period of time. The results are expressed as the water uptake per unit area. Thus, the mass was divided by the length and width of the bottom contact surface to obtain the total water uptake per square meter. The gradient, as determined by EN 13057 is defined as the sorption coefficient S [$kg{\cdot}m^{-2}{\cdot}h^{-0.5}$]. The weight of absorbed water is in such a way expressed as a coefficient indicating the tendency of the specimen to allow water penetration by capillary action. The samples were weighed before and after 5 min, 15 min, 30 min, 1 h, 2 h, 4 h, 8 h and 24 h of water contact.

2.4. Neutron radiography

Cracked specimens used for the neutron radiography measurements, consisted of another three 160 × 20 × 40 mm^3 samples per test series (sample composition and healing condition). The samples were conditioned after healing in the same way as mentioned in Section 2.3. The samples were transported to the neutron measuring station in sealed conditions (plastic foil) during 24 h.

The beam used for measuring the water penetration was the neutron beam line at the measuring station NEUTRA, the thermal neutron radiographic facility at the Swiss spallation source SINQ of the Paul Scherrer Institute (PSI) [51]. The proton current was approximately 970–980 μA with a peak energy of 25 meV throughout all tests. The neutron beam travelled through the studied object and hit the 100 μm LiF/ZnS scintillator screen as neutron-to-light converter. Then it hit a mirror in the dark room and was recorded by a CCD camera, a cooled slow-scan Andor SCMOS camera with a 50 mm AF-S NIKKOR lens. The recording resulted in a radiograph consisting out of an array of grey level intensity values. The pixel size obtained with an exposure time of 20 s was 138.89 μm/pixel.

Per test run, a maximum of ten samples were placed on line supports into five water basins mounted on a support frame (Fig. 1). First, dry reference images were taken before the containers were filled with water. Subsequently, water was added manually 3 min before the actual start of neutron radiography. The samples were approximately 4 mm immersed in the liquid. Post-processing revealed an immersion of 4.12 ± 1.00 mm. Subsequent radiographs were made for a total measuring time of 2 h. In this way, the water penetration due to capillary suction in the cement-based material could be followed as a function of time. The relation between the intensity values and composition of the sample is described by the law of exponential attenuation, also known as the Beer-Lambert law (Eq. 1). The wet and dry radiographs were compared to each other and the water content could be calculated quantitatively (Eq. 2–6) by logarithmically dividing the wet and the dry state and multiplying this value by the density of water and dividing it by the attenuation coefficient of water and the thickness of the sample.

$$I = I_0 \bullet e^{-\Sigma \bullet d} \tag{1}$$

$$I_{dry} = I_0 \bullet e^{-\Sigma_{dry} \bullet d} \tag{2}$$

$$I_w = I_0 \bullet e^{-\Sigma_{dry} \bullet d - \Sigma_w \bullet d_w} \tag{3}$$

$$W = \frac{\rho_w \bullet V_w}{V} = \frac{\rho_w \bullet d_w}{d} \tag{4}$$

$$I_{wet} = I_{dry} \bullet e^{\frac{-\Sigma_w \bullet W \bullet d}{\rho_w}} \tag{5}$$

$$W = -\frac{\rho_w}{\Sigma_w \bullet d} \bullet ln\left(\frac{I_w}{I_{dry}}\right) \tag{6}$$

where I is the flux through a sample [$cm^{-2}{\cdot}s^{-1}{\cdot}\mu A^{-1}$], I_0 the flux penetrating into the sample [$cm^{-2}{\cdot}s^{-1}{\cdot}\mu A^{-1}$], Σ the attenuation coefficient [cm^{-1}], d the thickness of the sample [cm], I_{dry} the flux transmitting through dry material [$cm^{-2}{\cdot}s^{-1}{\cdot}\mu A^{-1}$], I_w the flux through wet material [$cm^{-2}{\cdot}s^{-1}{\cdot}\mu A^{-1}$], Σ_{dry} the attenuation coefficient of dry material [cm^{-1}], Σ_w the attenuation of water [3.64 cm^{-1}], d_w the thickness of the observed water layer [cm], W the water content [$kg{\cdot}m^{-3}$], ρ_w the density of water [$kg{\cdot}m^{-3}$], V_w the volume of water [m^3] and V the volume of the sample [m^3].

Before the start of the capillary absorption tests, the specimens were weighed with a Sartorius BP 3100 S balance (0.01 g accuracy). After the 2 hour test, the wet mass was determined using the same mass scale. The total amount of absorbed moisture was quantified and compared to the value obtained by post-processing the neutron radiographs.

First, each radiograph obtained with neutron radiography needed to be filtered with the image correction tool “Quantitative Neutron Imaging” (QNI) [52] for qualitative and quantitative information. Several deviations on the attenuation were taken into account. The images were corrected using the dark current, the open beam (flat field) and the black body radiographs. These separate radiographs were made before every new test series. The dark current is a radiograph where all shutters of the beam were closed. The open beam shows a radiograph with the spatial distribution and inhomogeneity of the neutron beam intensity as a measure for the background noise. The black body radiograph was made when boronated polyethylene blocks were placed in front of the samples. These blocks are able to absorb the neutrons and gave an estimate of the background scattering correction. All corrections were based on an average of five radiographs per correction factor, to further optimize the obtained results.

All further image operations were performed using the image processing software ImageJ. After post-processing of the radiographs, the measured wet states images were divided by the dry state images as a qualitative measurement of the moisture distribution and content. The dry states were calculated by averaging five subsequent dry images. The total water content in the not-immersed part of the sample was calculated. The part which was immersed was assumed to have a water content equal to the immediately adjacent part just above the water level obtained after 2 h of capillary water absorption through the cementitious matrix. This amount was added to the already obtained value of the total water content of the not-immersed part of the sample. As water was present in front of and behind the specimen, using the initial darker value for the immersed part would result in higher and false quantitative measurements.

Furthermore, two distinct water content profiles along the

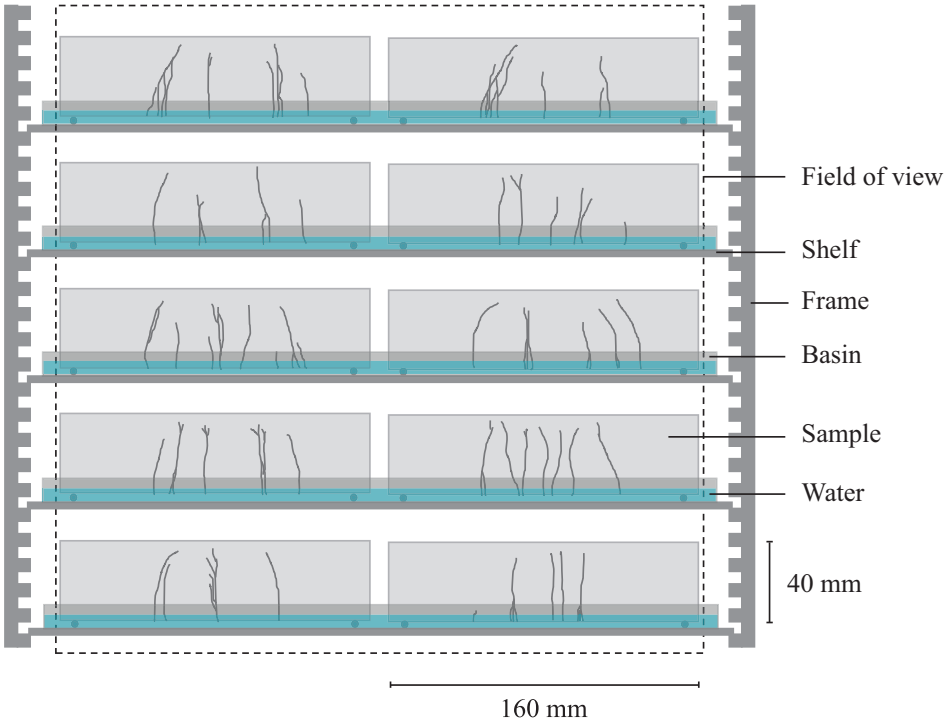

Fig. 1. Experimental setup showing the 20 × 40 × 160 mm^3 cracked samples immersed in approximately 4 mm of water for capillary absorption during neutron radiography. Ten samples were placed on 5 shelfs mounted on a frame. The dashed lines show the field of view during neutron radiography measurements.

horizontal axis were calculated using a rectangle grey-level profile plot:

1) Adjacent to the water level but not immersed;
2) At approximately two thirds of the total height of the specimen.

In this way the water movement in time could be studied and visualized in detail. The profiles were made at 5 min, 10 min, 15 min, 45 min and 2 h in measuring time.

3. Results and discussion

In this section, the observed characteristics of the REF and SAP samples are discussed (Section 3.1). These include the stress-strain diagrams and the observed visual closure of the multiple cracks by means of microscopic analysis. Next, the capillary absorption as calculated by means of image analysis on the neutron radiographs are compared to the results obtained with gravimetric capillary water absorption tests (Section 3.2). In the end, the different obtained water profiles are discussed in detail. The water penetration through cracks towards the cementitious matrix is discussed (Section 3.3).

3.1. Material characteristics: Mechanical properties and visual closure

The typical obtained stress/strain curves are shown in Fig. 2. In these curves, upon loading, the stress increases till the point of first cracking. This can be seen as a small drop in stress at about 0.5% to 0.7% strain (as depicted with arrows on the top curve). After this first crack, the synthetic microfibres are pulled out and are able to take over the additional stresses in the material as they are bridging the cracks. The progression in crack width increase is thus stopped and the cementitious material is forced to crack somewhere else upon stress increase. Therefore, another crack is formed, but again, fibres are able to deal with the increased load and the material will be able to take up higher forces. In this way, not a single large crack, but multiple small cracks are formed due to this strain-hardening effect. These cracks are beneficial in terms of autogenous healing as the crack widths are limited to 50 μm to 60 μm due to the proper mixture design. If the material would be loaded further the weakest crack would open, leading to a complete failure of the composite. This is called strain-softening. The fibres are no longer able to cope with the additional forces and are completely pulled out or experience failure.

In the curves in Fig. 2, the stresses increase and several drops (multiple crack formations) are seen. The first-cracking-strength amounts to 6.3 ± 0.6 MPa for REF samples and 5.9 ± 0.4 MPa for SAP samples. These are typical values for such kind of strain-hardening materials [19] and the difference between SAP and REF samples is not statistically significant. All samples were pre-loaded till 2.5% strain and upon unloading, this value decreased to approximately 1.8%. The ultimate strain is 3–4% [37], so the serviceability limit state crack widths are studied. The SAP samples would even show a more pronounced strain-hardening effect, compared to the REF specimens, as the SAP particles act as stress initiators [53], helping in the formation of multiple cracks. These specimens show a higher possible strain compared to REF samples. The observed crack widths are comparable between the REF and the SAP samples.

When studying the compressive strength of the materials, REF samples show a compressive strength of 77.4 ± 1.2 MPa and SAP specimens (with 1 m% of cement weight SAP) 67.0 ± 1.4 MPa. This means a reduction of 15.6% in compressive strength. However, this strength suffices for most applications. The strength reduction is due to a dual effect. First of all, there is a positive effect of internal curing [29], but this is combined with a negative effect of macro pore formation [49, 54] reducing the cross-sectional area and thus the overall strength. For the first-cracking-strength both effects balance each other while for the compressive strength the influence of the macro pore formation seems to be more pronounced. The amount of 1 m% was based on previous research to get optimal sealing [36] and healing [22, 24, 37]. A further increase in SAP content would lead to a detrimental effect of the macro pores on the mechanical properties and thus huge strength losses.

When studying the formed healing products, it was clear that when being exposed to wet/dry cycling, the cracks were able to close to full extent (Fig. 3), both in REF and in SAP samples. The healing products

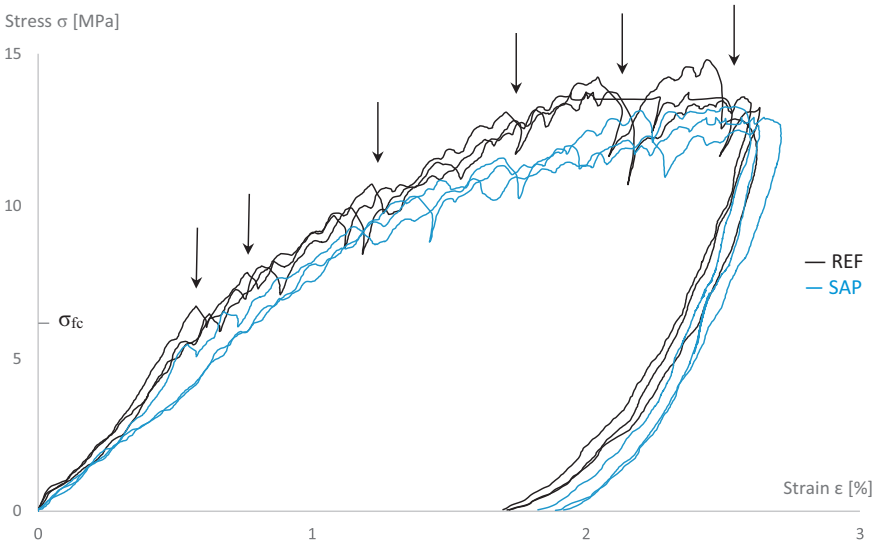

Fig. 2. Typical stress strain curves of the 20 × 40 × 160 mm^3 samples loaded till 2.5% strain using four-point-bending. Both series show a first-cracking strength σ_{fc} around 6 MPa. A clear strain-hardening effect with multiple crack formation (as depicted by arrows on clear stress drops) is observed.

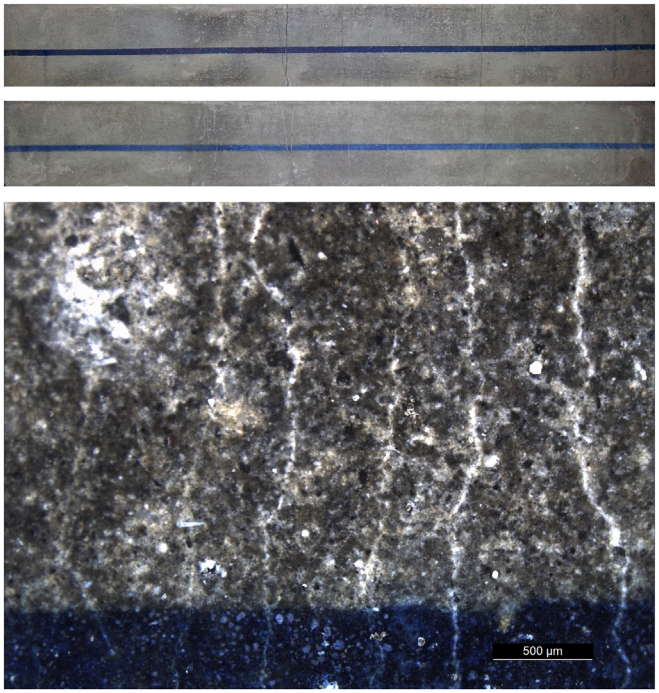

Fig. 3. Visual closure on the bottom of samples after being healed for 28 days in wet dry cycling. Clear further hydration and calcium carbonate crystallization can be seen. The scale bar on the bottom part of the figure amounts to 500 µm.

are formed due to a combination of further hydration, pozzolanic activity of the fly ash, and the formation of whitish calcium carbonate crystals. Fig. 3 shows the performance of a strain-hardening material in terms of autogenous healing. Small multiple cracks show complete healing (30–50 µm) [18, 24]. As the crack widths are limited, the amount of building blocks and healing products is sufficient. A larger crack would not be healed as effectively (partial healing up to 150 µm) [18, 24]. So, when comparing these multiple, small, but healable cracks with a single, large and unhealable crack, the former condition has the preference.

In an environment with a relative humidity of > 90%, only the samples with SAPs show partial healing, mainly due to further hydration in a kind of stitching pattern. As the SAP particles are also able to absorb moisture even without being into direct contact with liquid water [50], they are able to stimulate autogenous healing as well at sufficiently high relative humidity [24]. Especially in the interior of the sample, these formed healing products play an important role. As near the crack tip the crack width is much smaller compared to the one at the crack mouth, limited healing products may already bridge a crack locally. This leads to physical blocking of the crack and possibly also in a regain of mechanical properties [22, 24]. In wet/dry cycles, the healing mostly occurs near the crack mouth (to 700–1000 µm below the crack mouth [23]). Most of this healing occurs in the first three to seven wet/dry cycles. As the crack is sealed quite quickly, the healing in the interior of the sample is partially inhibited. This may have a consequence for the water penetration in a crack. Therefore, in this paper, we aimed at investigating the water profiles in these materials by means of neutron radiography (see later on).

The crack closure in percentage as measured by comparing the crack widths before and after 28 days of healing is shown in Fig. 4. In all samples, the crack widths were limited to approximately 60 µm. By studying this figure, it is clear that no healing was observed in REF samples stored at a relative humidity condition higher than 90%. This absence of healing would be the same when storing the samples at a RH of 60%. When SAP samples were stored at 60% RH conditions, limited healing was observed. At > 90% RH, partial visual closure was observed in the form of further hydration. Especially in the interior of the sample [23], this healing could lead to the observed regain in mechanical properties [24]. The main cause for this healing is the ability of SAPs to absorb moisture from the environment. They are able to absorb up to 3 to 4 times their weight in moisture [50]. This already seems to be sufficient for stimulating and promoting autogenous healing in the vicinity of the SAP particles.

When subjected to wet/dry cycles, the healing of REF samples was more pronounced compared to the samples stored at high RH conditions. Cracks up to 30 µm are able to close completely. Larger crack widths are able to partially close. It was clear that in SAP specimens, this healing was even more pronounced compared to the REF samples. As SAPs are able to retain water in their structure, water is also available during the dry periods and optimal conditions for autogenous healing are present. In this way, they stimulate and promote autogenous healing. Larger crack widths are able to close and an improved healing is observed. The results are in correspondence to results obtained with X-ray microtomography [23]. In the latter research, only the outer 700–1000 µm are completely sealed by healing products. This optimal healing leads to the regain in mechanical properties [24] and to

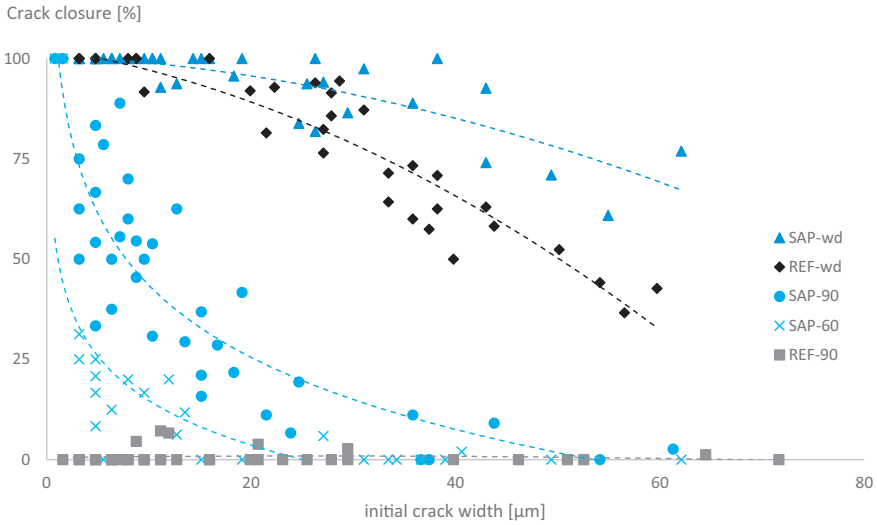

Fig. 4. Percentage of visual closing found in the observed cracks for every test series. The crack widths were limited to approximately 60 µm. More healing is observed in healing conditions with liquid water present.

a possible regain in water tightness. But, the extent of this healing, especially in the interior of the cementitious material, is still object of discussion and was therefore studied further on in the next section.

The autogenous healing leads to a regain in mechanical properties [22, 24]. The healed specimens are able to regain some of their mechanical properties (up to 75%). Even second reloading of those healed samples leads to partial additional regain in mechanical properties (up to 66%) [22].

3.2. Capillary absorption using gravimetric analysis and neutron radiography

The masses as obtained with image analysis of the neutron radiographs and as obtained with mass-scale measurements (after 2 h of capillary absorption) are shown in Fig. 5 as an average of the neutron radiography measurements on three different samples. A good statistical correlation exists between both measurement techniques, showing the positive aspect of neutron radiography as a quantitative measurement technique. The small difference may be due to the assumption that the water content in the immersed part of the samples is the same as the water content just above the water level (see Section 2.4).

From Fig. 5, it is clear that more water is absorbed by less healed specimens and less water is absorbed by healed specimens. In order of decreasing amount of absorbed water; SAP specimens at a RH of 60%, REF samples at a RH > 90%, SAP samples at an RH > 90% (−45% compared to REF-90), REF samples in wet/dry cycles (−52% compared to REF-90) and SAP samples in wet/dry cycles (−75% compared to REF-90). The latter shows almost no absorption compared to the other test series. Furthermore, there seems to be a good correlation with Fig. 4 which shows the percentage of visual closure of the initial cracks. If the healing is better, the absorbed water content is lower. This means that the (promoted) healing of the cracks is important in terms of the capillary water absorption. It has to be mentioned that the SAP particles are storing their absorbed water when measuring the mass of the samples. Taking this into account, the value in the matrix itself is even lower.

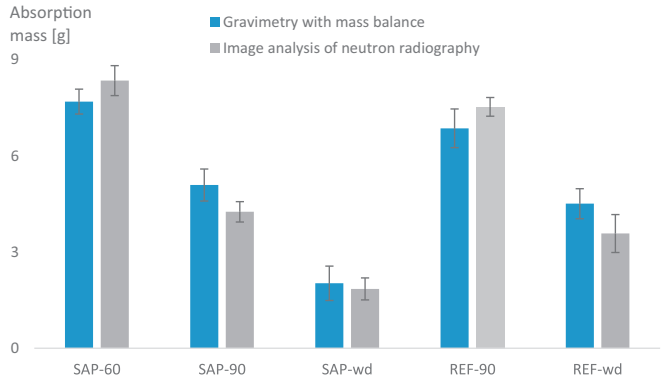

Fig. 5. Comparison between the masses obtained by gravimetric mass balance measurements and by image analysis of the obtained and corrected neutron radiographs, both at 2 h of capillary absorption. Both masses are comparable.

It would be interesting to study the absorption of water as a function of time. When all radiographs are studied and analysed, Fig. 6a is obtained. Here, the mean water absorption in grams is shown together with the standard deviation on the single results (n = 3). The averages undergo small deviations with respect to the general trend for the different test series. This is due to fluctuations of the neutron beam itself. The current needs to be constant as a function of time to get uniform images, but sometimes the proton current decreases due to sudden failure of the beam. These images thus showed a slight decrease in overall dose. The average proton current was 970–980 µA, but the threshold value was 900 µA. Generally, these observed fluctuations are minor compared to the deviation on the water penetration itself, so the different test series could be compared.

As a function of the square root of time, the overall absorbed mass increases. The conclusions drawn earlier, based on the water absorption after 2 h (Fig. 5), are confirmed. The highest amount of water is absorbed by REF samples stored at a relative humidity condition of > 90%, closely followed by the SAP specimens stored at a RH condition of 60%. There seems to be an increase in water uptake rate for the SAP samples compared to the REF specimens. Then, there is a significantly lower amount of absorption by the SAP specimens at > 90% RH and the REF specimens stored in wet/dry cycling. The SAP specimens stored in wet/dry cycles show the best results in terms of impermeability. Here, the water absorption rate is very low and only a minor increase in mass absorption is observed in time. Even though the scatter is noteworthy due to the cracked nature of the samples and the healing, differences in absorption could be noticed.

The results obtained with neutron radiograph analysis seem to correspond perfectly compared to the results obtained by capillary water absorption measurements (Fig. 6b). In time, the absorption rate seems to be comparable. The same conclusions can be drawn. However, when looking at the results obtained from neutron image analysis, the

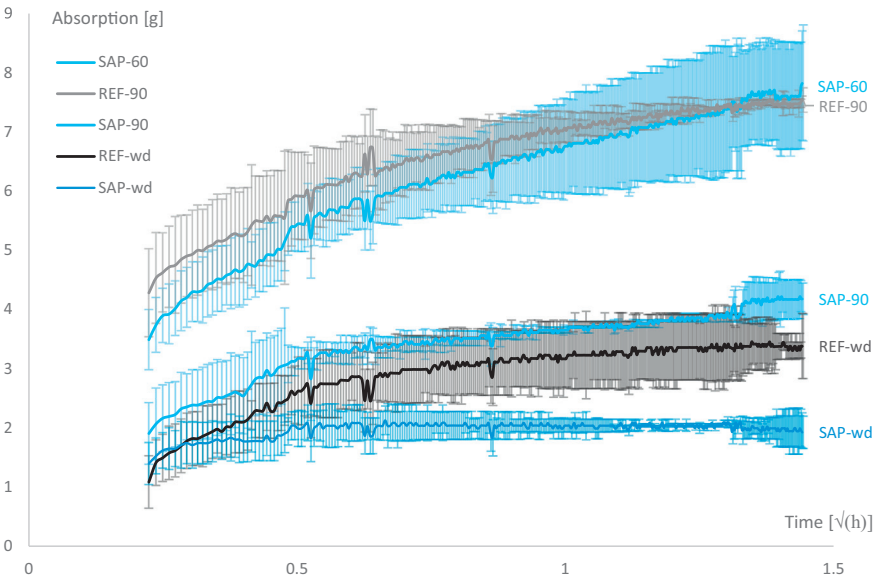

(a)

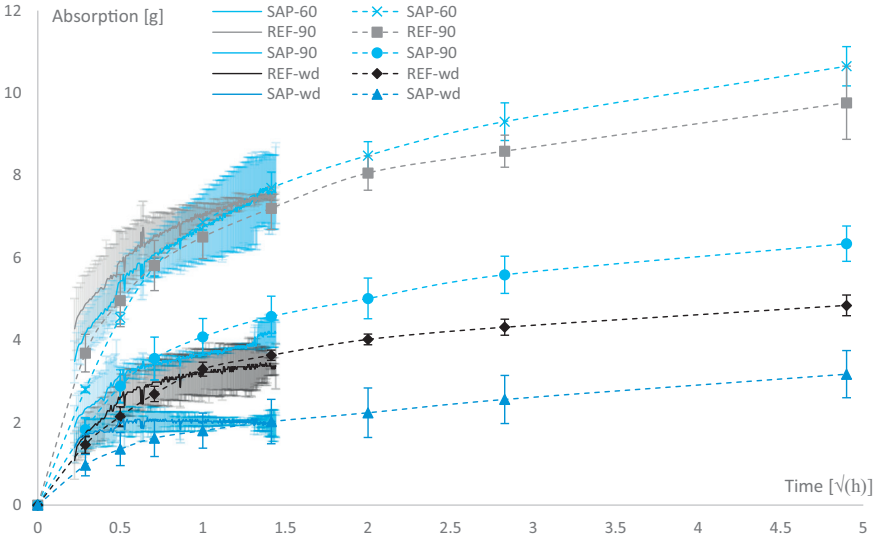

(b)

Fig. 6. Capillary water absorption [g] as a function of the square root of time [√(h)] showing the increase in mass in the cracked healed specimens using image analysis on the neutron radiographs **(a)**. The lower the curve, the better the sealing and/or healing capacity. Comparison between the obtained results by image analysis of neutron radiographs (solid lines) and the capillary water absorption mass method following the Standard EN 13057 (dashed lines) **(b)**.

initial absorption seems to be higher. This is due to the assumption that the immersed part of the specimen would have a water content equal to the water content just above the water level after 2 h of water absorption test. This may not be true. As the mixture is a self-compacting and quite dense mixture, the water penetration could be more delayed in time. However, when penetration in cracks accounts for the largest part of the absorbed mass of water, this assumption is of less importance. If the assumption would not be made and only the upper part of the sample would be studied, an underestimation would be made. When looking at the results from 1 h onwards, the trends obtained from neutron radiography are the same as when using capillary absorption tests. After 24 h of capillary absorption testing, the mass gain amounts to 10.7 ± 0.5 g, 9.8 ± 0.9 g, 6.3 ± 0.4 g, 4.8 ± 0.2 g and 3.2 ± 0.6 g for SAP 60% RH, REF > 90% RH, SAP > 90% RH, REF wet/dry cycles and SAP wet/dry cycles, respectively. The specimens showing limited crack healing started to become more and more saturated.

When one would divide the mass by the exposed contact surface (which is 160 × 20 mm^2), the absorption per square meter can be obtained. Using the standard EN 13057, the sorption coefficient could be calculated. This coefficient represents the ability to absorb water due to capillary suction. The sorption coefficients for the test series were 0.68 ± 0.03 $kg{\cdot}m^{-2}{\cdot}h^{-0.5}$, 0.40 ± 0.03 $kg{\cdot}m^{-2}{\cdot}h^{-0.5}$, 0.20 ± 0.04 $kg{\cdot}m^{-2}{\cdot}h^{-0.5}$, 0.62 ± 0.06 $kg{\cdot}m^{-2}{\cdot}h^{-0.5}$ and 0.31 ± 0.02 $kg{\cdot}m^{-2}{\cdot}h^{-0.5}$ for SAP = 60% RH, SAP > 90% RH, SAP wet/dry, REF > 90% RH and REF wet/dry, respectively. Even though cracked samples are tested, the results show that the SAPs are able to prevent water penetration in cracked cementitious materials. The results are closely linked to the visual crack closure observed by microscopic analysis.

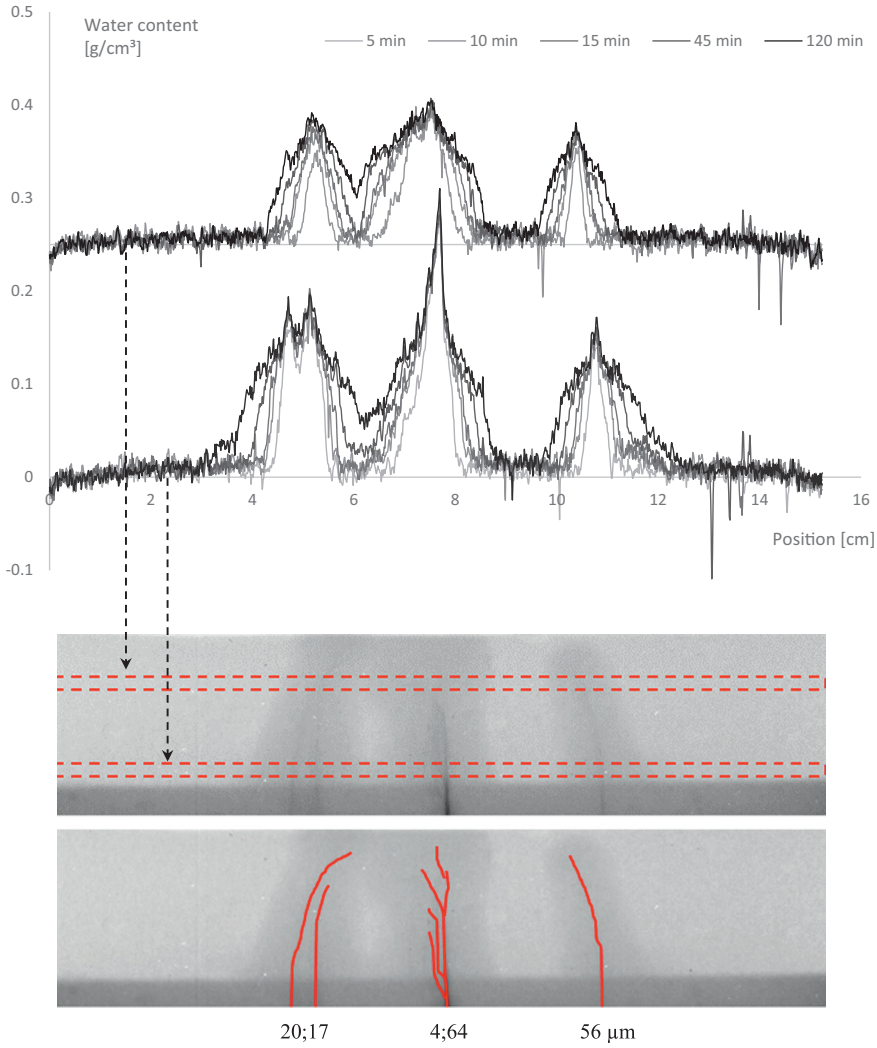

Fig. 7. The water content [g/cm^3] above the level of submersion and at two thirds of the total height in *REF specimens healed at a RH of > 90%* showing three distinct cracks and a clear and high water uptake through the cracks. The top water profiles are shifted upwards with a constant 0.25. The water profiles show the water content after 5 min, 10 min, 15 min, 45 min and 120 min of water contact, respectively. As a reference, the locations of the studied rectangles (dashed lines) and the observed visual cracks by means of microscopy are shown beneath the water profile curves. The measured initial crack widths are shown underneath the respective cracks.

3.3. Obtained water profiles for the different test series

Figs. 7–11 show typical results for the obtained water profiles using neutron radiography after 5, 10, 15, 45 and 120 min of water contact. The water profiles of all samples of the different test series are provided as Supplementary material. Generally, when looking at the cementitious matrix itself, it is clear that the water front only gradually progresses due to capillary action. In a crack, this water front quickly intrudes the matrix leading to an increase of the observed grey values and thus absorption in time (see results in Section 3.2). Two different locations were studied, being right above the water level and at a height of approximately two thirds of the total height. These locations are also shown on the radiograph after 2 h of capillary absorption testing by means of a dashed rectangle. To be complete, the visually observed crack pattern by means of microscopic analysis is depicted as well (red lines). The clear peaks in the water profiles correspond to the locations of the cracks themselves. The combinatory approach of studying the cracks visually and together with water profiles leads to solid conclusions in terms of the observed healing of the cracks and water penetration through them. In that way better conclusions can be drawn about the water penetration in the interior of the specimen, after being healed.

When looking at the results for the REF samples stored in a relative humidity condition of > 90% (Fig. 7), it is clear that there is a vast ingress of water through these cracks. Even after 5 min of contact time, the ingress is already substantial. The water penetration through the cracks towards the cementitious matrix further increases as a function of time. On the left hand side a double crack is found as two clear peaks are seen in the lower water content profile. In the upper part, the effect of both cracks is combined. It is clear that this double crack leads to more water ingress compared to the single crack observed on the right hand side. As there is no healing of the crack (see Section 3.1), water is not inhibited to move in the cementitious matrix through the cracks. This is not beneficial in terms of durability and therefore unwanted. The sample quickly becomes saturated. The water movement from a crack towards the cementitious matrix propagates inwards over approximately 3 mm, 4 mm, 5 mm, 7 mm and 10 mm after 5 min, 10 min, 15 min, 45 min and 2 h in the lower rectangle. In the upper rectangle, this is approximately 1 mm, 2 mm, 3 mm, 4 mm and 6 mm, respectively.

For the REF specimens stored in wet/dry cycles (Fig. 8), the water movement is only partially prevented by the healed cracks. The cracks are still clearly seen as peaks in water content. The peaks in the upper part of the sample are masked as less water is penetrating through the cracks. The rate of water penetration in the cementitious matrix is also lower compared to the unhealed REF samples. The distances of penetration in the lower part are approximately 2 mm, 3 mm, 4 mm, 5 mm and 6 mm after 5 min, 10 min, 15 min, 45 min and 2 h of testing. This is already lower compared to unhealed specimens, but still noteworthy.

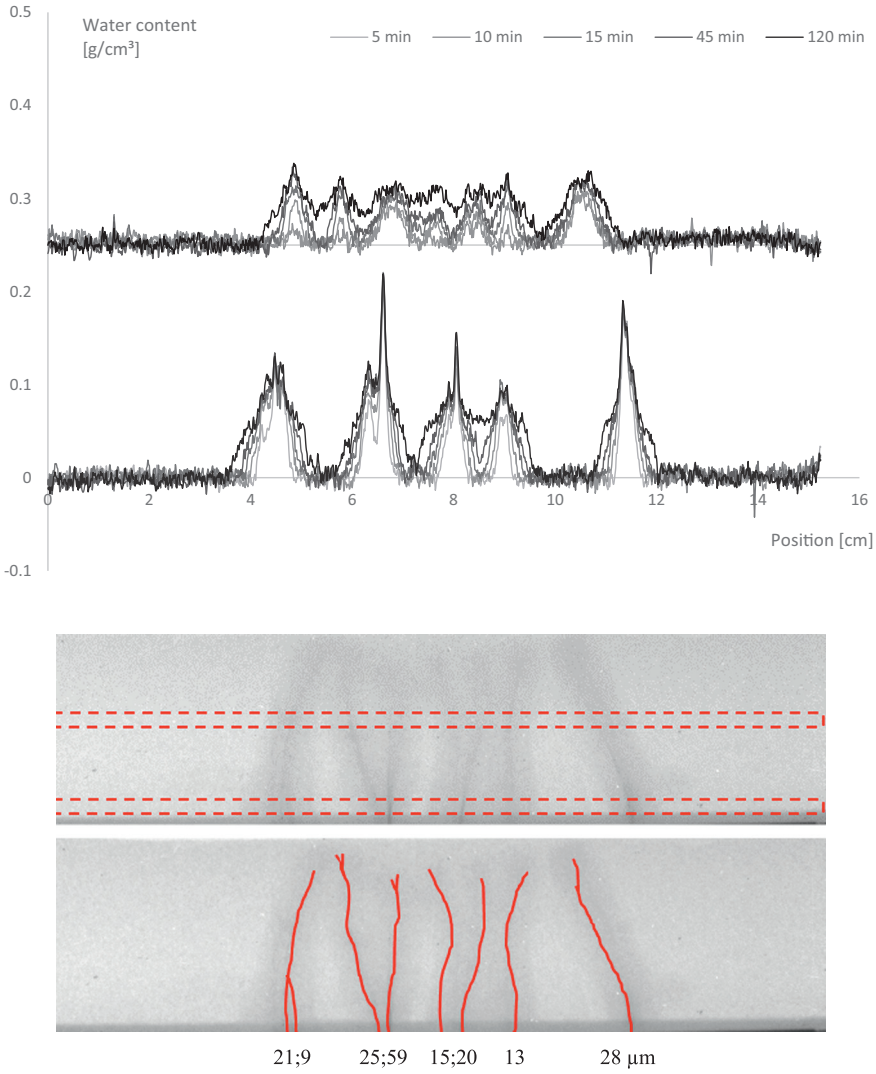

Fig. 8. The water content [g/cm^3] above the level of submersion and at two thirds of the total height in *REF specimens healed in wet/dry cycling* showing five distinct cracks and a partial water uptake in healed cracks. The top water profiles are shifted upwards with a constant 0.25.

Samples with SAPs may show better results. Not only is the healing in REF samples of inferior quality compared to the healing in SAP samples, the SAP are able to swell and physically block a crack for intruding fluids. In the upper region of the REF samples, the absorption is delayed with half an hour approximately. The grey levels are lower compared to the case where the specimens' cracks would not have healed properly. This vaguer color shows that only part of the crack is prone to water penetration and thus that the healing action was not entirely sufficient.

For the SAP specimens stored at a RH of 60% it is clear that a quick ingress of water is observed (Fig. 9). Capillary action is also observed in the higher regions. In the left crack, the capillary action is only visible after 10 min of testing. Partial blockage by the SAPs may be the reason for the delay. As the SAP particles are able to swell, they will physically hinder the water moving further in the crack. From the crack, a clear horizontal movement can be seen as well. On the right hand side, a double crack is found, as was the case for the REF samples at > 90% RH. Even though the ingress is still substantial, the swelling action of the SAPs partially prevents water movement through the cracks, as compared to REF samples. In this study, the width is substantially lower compared to the 200 µm wide cracks studied in previous research [36]. There thus was a very fast capillary action and the SAP particles seemed not able to perfectly seal a crack upon water intrusion. The swelling of the SAPs into the crack is also somewhat hindered due to the smaller crack. Capillary action is still prominent even though SAPs are able to swell as water may be absorbed in between single SAP particles. When studying the water permeability in cracks of larger magnitude, the SAPs are able to seal a crack for further intrusion of water flow [36] as they are partially deformed in a crack, i.e. they are able to change form to small extent.

The water penetration from the cracks into the cementitious matrix occurs at the same rate as for unhealed REF samples. The healing in SAP samples was still too low to seal cracks physically by healing products. The rate of water intrusion in the cementitious matrix for REF and SAP samples is the same as the cementitious matrix shows the same effective water-to-cement ratio and microstructure [49, 50]. Even though the SAPs are able to swell within their formed macro pores, the water movement through the same overall microstructure in between the macro pores is the same.

For SAP samples stored at a RH of > 90% (Fig. 10), the ingress of water is further delayed and the total absorbed water mass is less compared to the SAP specimens at 60% RH. The rate of water penetration in the cementitious matrix is again comparable. The healing of only narrow cracks may have an influence, as the larger cracks were not healed effectively (see Section 3.1). The smaller middle crack only

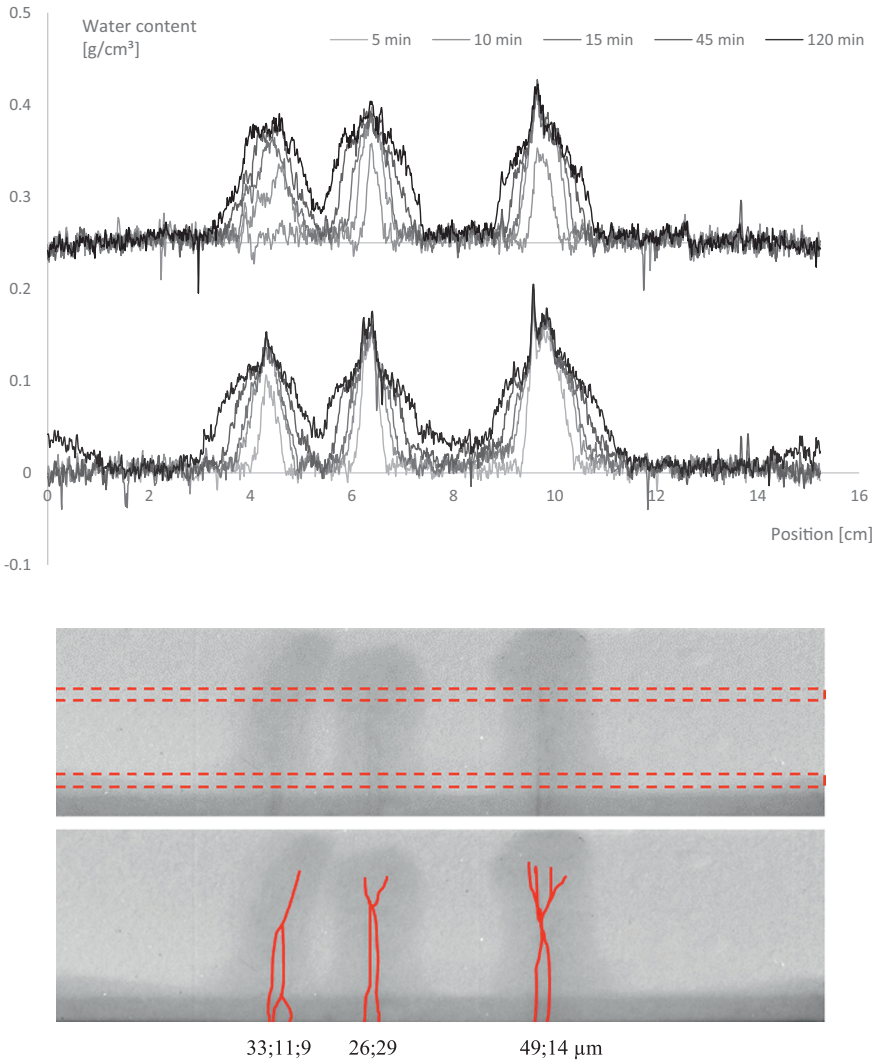

Fig. 9. The water content [g/cm^3] above the level of submersion and at two thirds of the total height in *SAP specimens healed at a RH of 60%* showing three distinct cracks and high water penetration through the cracks. The top water profiles are shifted upwards with a constant 0.25.

shows water penetration after 10 min of testing. It does not show the presence of water in the upper regions. This crack seems to be healed partially and the water movement is prevented along the height. The stimulated healing action by the SAPs leads to this feature. The delay in water penetration may be due to slower capillary action through a partially healed crack. The crack does not progress as high as the other observed cracks and this may lead to the absence of water in the upper rectangle. The smallest crack at the right hand side, however, does not show any kind of water penetration whatsoever. Only a small increase at the 12 cm position is noticed. This crack (6 µm) was small enough to be healed completely.

When studying the results of the SAPs samples exposed to wet/dry cycling, it is obvious that the healing of the cracks prevented further ingress of water in the cracked matrix (Fig. 11). Even though several cracks were formed, only two distinct cracks are seen in the lower profiles, while only one single crack is seen after 120 min of testing in the upper curves. The water profile of the upper part progresses through the crack. In the right crack, the water movement is also very slow and the water front moves vertically in time, comparable to the horizontal movement of the water as in all other test series. The rate is the same. Here, the healing together with the blocking effect of the SAPs in the interior prevent further movement of water in the crack, thus leading to a regain in impermeability. In the two left cracks, perfect healing was observed. The healing at the crack mouth seemed to be efficient in counteracting the water ingress.

In REF specimens exposed to > 90% RH the penetration and amount of water is highest compared to all test series. As there is no hindrance for water penetration, when coming into contact with water, the crack immediately fills with water. In order to prevent corrosion of the reinforcement (especially when the fluid contains dissolved chlorides), it is important that the water penetration does not reach the reinforcement. Unhealed specimens show a high capillary rise of water in the cracks which should be avoided. In the healed specimens, some cracks are efficiently sealed with healing products, preventing the ingress of water. SAPs further aid in hindering the water movement as they are able to swell and block a crack if water comes into contact with the polymer. The time at which corrosion may start is thus delayed. These aids in the possible increase in durability and the possible longer service life of structures built with a strain-hardening materials and incorporated superabsorbent polymers.

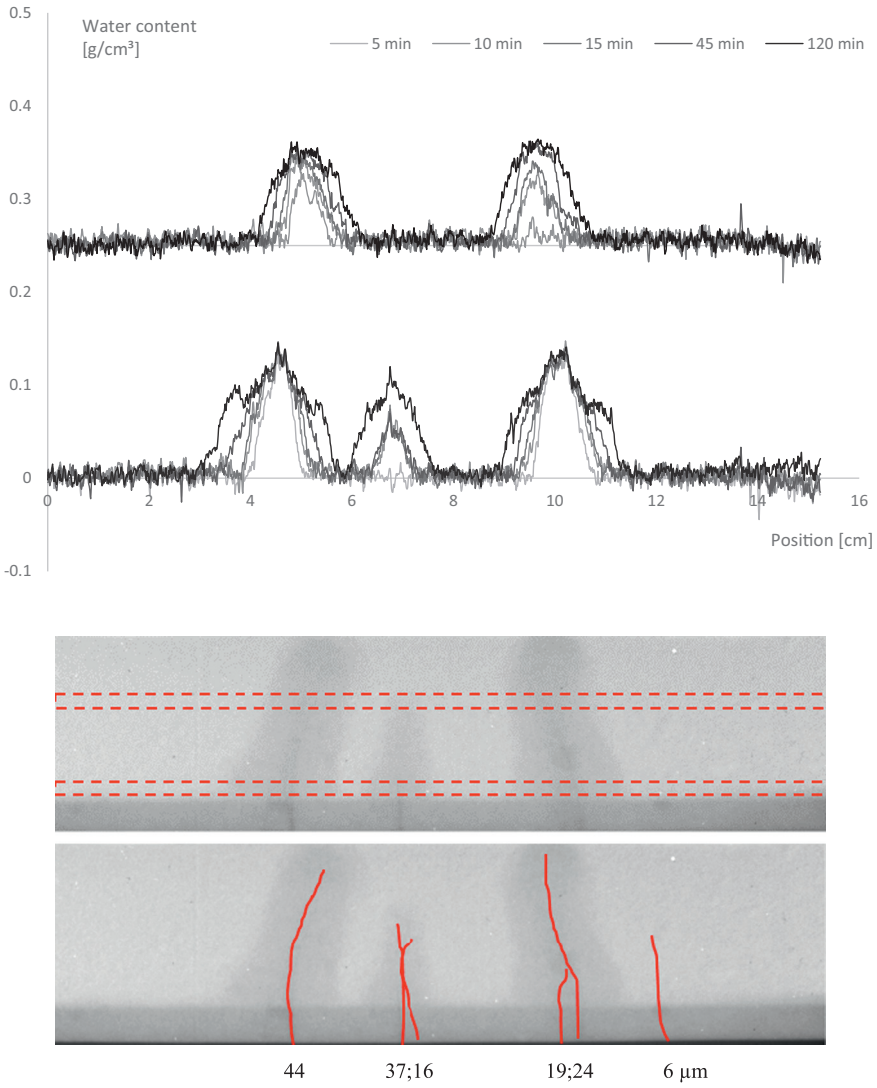

Fig. 10. The water content [g/cm^3] above the level of submersion and at two thirds of the total height in *SAP specimens healed at a RH of > 90%* showing three distinct cracks and a partial blockage of water uptake. The top water profiles are shifted upwards with a constant 0.25.

4. Conclusions

Based on the findings of the research on the permeability of cementitious materials with and without SAPs as studied by means of neutron radiography following conclusions can be drawn:

- The best healing was obtained for SAP samples exposed to wet/dry cycles, followed by REF exposed to wet/dry cycles, SAP at a relative humidity of > 90%, SAP at a relative humidity of 60% and REF at a relative humidity of > 90%.
- In high relative humidity condition the REF specimens do not show healing in any kind of form as there is no presence of liquid water. When being exposed to wet/dry cycles, these REF samples show clear visual closure of cracks up to 30 µm.
- The SAPs are able to stimulate and promote autogenous healing, even at high relative humidity conditions of > 90%.
- Healing of specimens with SAPs in a relative humidity condition of > 90% is comparable to the healing of REF specimens exposed to wet/dry cycles. When subjected to wet/dry cycles, the SAP specimens show a pronounced healing and cracks larger than 50 µm also show some extent of healing.
- Neutron radiography is a powerful tool to visualize and quantify the moisture profiles in cracked cementitious materials. The results are comparable to the gravimetrical analysis of the capillary absorption in time.
- Compared to REF stored in a relative humidity of > 90%, REF exposed to wet/dry cycles shows a decrease of −52% in absorbed mass, SAP at a RH > 90% a decrease of −45% and SAP in wet/dry cycles a decrease of −75% in absorbed water mass.
- When studying the reference material without SAPs in a relative humidity condition, the water penetration is high and this is unwanted in terms of durability aspects. The water penetration should be prevented or counteracted.
- SAPs are able to cause a regain in impermeability and the water movement is partially counteracted. The ingress is delayed in time due to the swelling action of the SAPs.
- As the healing is more pronounced in SAP specimens, the cracks are also sealed in a better way compared to REF samples. This leads to a lower ingress of water through these cracks as the path is physically and pertinently blocked. The swelling action of the SAPs further aids in this mechanism as possible intruding water is inhibited from intrusion in the cementitious matrix.

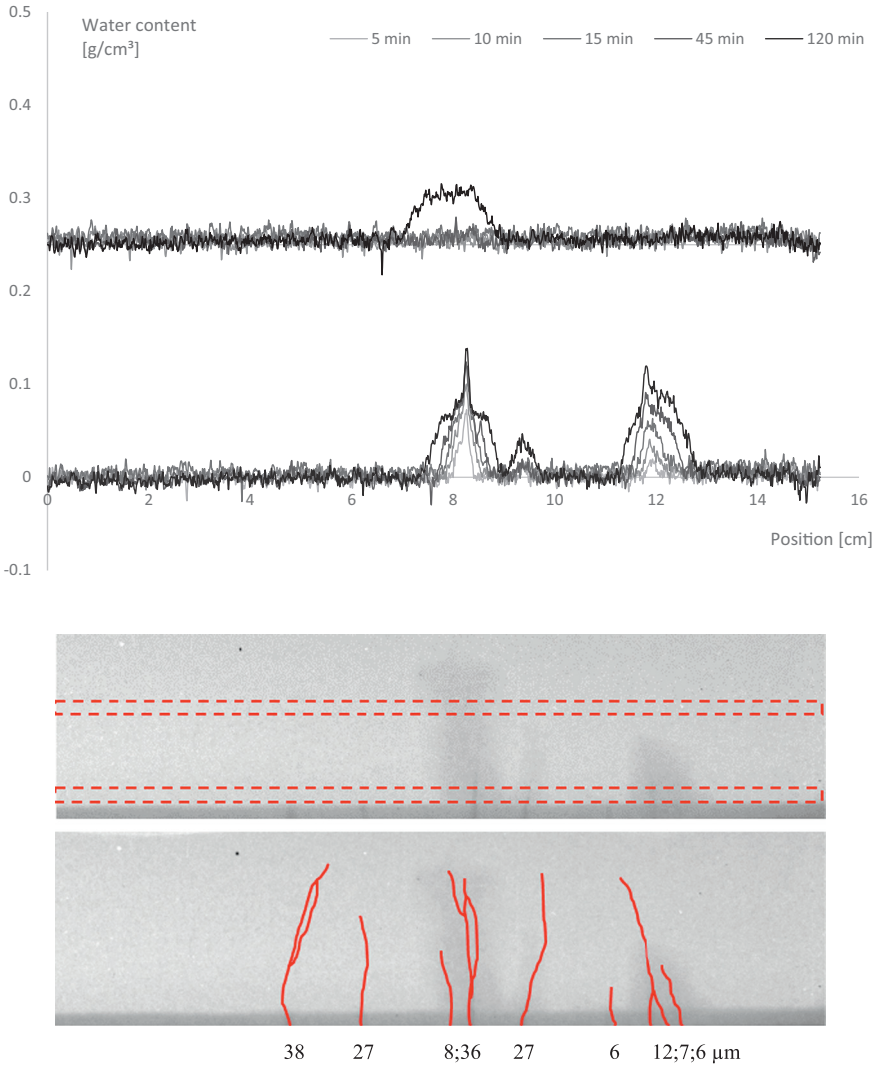

Fig. 11. The water content [g/cm^3] above the level of submersion and at two thirds of the total height in *SAP specimens healed in wet/dry cycling* showing five distinct cracks and a low water uptake in healed cracks. Some cracks do not show any kind of water penetration. The top water profiles are shifted upwards with a constant 0.25.

– SAPs are a promising admixture to be used in a cementitious material for self-sealing and promoted autogenous healing. The durability may be enhanced as less fluids can penetrate the structure. This may lead to an increase in service life.

Acknowledgements

As a Postdoctoral Research Fellow of the Research Foundation-Flanders (FWO-Vlaanderen), D. Snoeck would like to thank the foundation for the financial support (12J3617N). The authors would like to thank the Paul Scherrer Institute (PSI) for granting neutron beam time at the NEUTRA SINQ facility to execute the research proposal (ID No. 20170327). The staff of the Paul Scherrer Institute (PSI), and especially Mr. J. Hovind, are gratefully acknowledged for the support and the useful discussions on and about neutron radiography. The help of Mr. D. Hillewaere from the Magnel Laboratory of Concrete Research during the measurements was also greatly appreciated. In addition, the authors want to thank Dr. A. Assmann and Dr. G. Herth from BASF for providing SAP B.

Conflict of interest statement

The authors declare no competing financial interests.

Data availability statement

The datasets generated during and/or analysed during the current study are available from the corresponding author on reasonable request. Supplementary material (water profiles for all samples) are available and submitted next to this manuscript.

Appendix A. Supplementary data

Supplementary data to this article can be found online at https://doi.org/10.1016/j.cemconres.2018.07.002.

References

[1] K. Van Tittelboom, N. De Belie, Self-healing in cementitious materials - a review, Materials 6 (2013) 2182–2217.
[2] K. Van Tittelboom, N. De Belie, D. Van Loo, P. Jacobs, Self-healing efficiency of cementitious materials containing tubular capsules filled with healing agent, Cem. Concr. Comp. 33 (2011) 497–505.
[3] K. Van Tittelboom, J. Wang, M.A. Gomes De Araújo, D. Snoeck, E. Gruyaert, B. Debbaut, H. Derluyn, V. Cnudde, E. Tsangouri, D. Van Hemelrijck, N. De Belie, Comparison of different approaches for self-healing concrete in a large-scale lab test, Constr. Build. Mater. 108 (2016) 125–137.
[4] C. Dry, Matrix cracking repair and filling using active and passive model for smart time release of chemicals from fibers into cement matrixes, J. Smart Mater. Struct. 3

(1994) 118–123.
[5] J. Wang, D. Snoeck, S. Van Vlierberghe, W. Verstraete, N. De Belie, Application of hydrogel encapsulated carbonate precipitating bacteria for approaching a realistic self-healing in concrete, Constr. Build. Mater. 68 (2014) 110–119.
[6] J. Wang, A. Mignon, D. Snoeck, V. Wiktor, N. Boon, N. De Belie, Application of modified-alginate encapsulated carbonate producing bacteria in concrete: a promising strategy for crack self-healing, Front. Microbiol. 6 (2015) 1–14.
[7] H.M. Jonkers, Self healing concrete: a biological approach, in: S. van der Zwaag (Ed.), Self Healing Materials an Alternative Approach to 20 Centuries of Materials Science, Springer, 2008, pp. 195–204.
[8] H.M. Jonkers, Bacteria-based self-healing concrete, Heron 56 (2011) 1–12.
[9] B. Dong, G. Fang, W. Ding, Y. Liu, J. Zhang, N. Han, F. Xing, Self-healing features in cementitious material with urea – formaldehyde/epoxy microcapsules, Constr. Build. Mater. 106 (2016) 608–617.
[10] A. Kanellopoulos, P. Giannaros, A. Al-Tabbaa, The effect of varying volume fraction of microcapsules on fresh, mechanical and self-healing properties of mortars, Constr. Build. Mater. 122 (2016) 577–593.
[11] E. Mostavi, S. Asadi, M.M. Hassan, M. Alansari, Evaluation of self-healing mechanisms in concrete with double-walled sodium silicate microcapsules, J. Mater. Civ. Eng. 4015035 (2015) 4015035.
[12] L. Ferrara, Crystalline admixtures in cementitious composites: from porosity reducers to catalysts of self healing, in: V. Mechtcherine, C. Schröfl (Eds.), International RILEM Conference on the Application of Superabsorbent Polymers and Other New Admixtures in Concrete Construction, RILEM Publications S.A.R.L., Dresden, 2014, pp. 311–324.
[13] L. Ferrara, V. Krelani, M. Carsana, A “fracture testing” based approach to assess crack healing of concrete with and without crystalline admixtures, Constr. Build. Mater. 68 (2014) 535–551.
[14] M. Roig-Flores, S. Moscato, P. Serna, L. Ferrara, Self-healing capability of concrete with crystalline admixtures in different environments, Constr. Build. Mater. 86 (2015) 1–11.
[15] S. Sangadji, E. Schlangen, Self healing of concrete structures - novel approach using porous network concrete, J. Adv. Concr. Technol. 10 (2012) 185–194.
[16] S. Sangadji, E. Schlangen, Mimicking bone healing process to self repair concrete structure novel approach using porous network concrete, Process. Eng. 54 (2013) 315–326.
[17] C. Joseph, A.D. Jefferson, B. Isaacs, R.J. Lark, D.R. Gardner, Experimental investigation of adhesive-based self-healing of cementitious materials, Mag. Concr. Res. 62 (2010) 831–843.
[18] Y. Yang, M.D. Lepech, E.-H. Yang, V.C. Li, Autogenous healing of engineered cementitious composites under wet-dry cycles, Cem. Concr. Res. 39 (2009) 382–390.
[19] V.C. Li, Engineered cementitious composites (ECC) – material, structural, and durability performance, in: E. Nawy (Ed.), Concrete Construction Engineering Handbook, CRC Press, 2008, p. 78.
[20] D. Snoeck, N. De Belie, From straw in bricks to modern use of microfibres in cementitious composites for improved autogenous healing – a review, Constr. Build. Mater. 95 (2015) 774–787.
[21] D. Snoeck, P.-A. Smetryns, N. De Belie, Improved multiple cracking and autogenous healing in cementitious materials by means of chemically-treated natural fibres, Biosyst. Eng. 139 (2015) 87–99.
[22] D. Snoeck, N. De Belie, Repeated autogenous healing in strain-hardening cementitious composites by using superabsorbent polymers, J. Mater. Civ. Eng. 04015086 (2015) 1–11.
[23] D. Snoeck, J. Dewanckele, V. Cnudde, N. De Belie, X-ray computed microtomography to study autogenous healing of cementitious materials promoted by superabsorbent polymers, Cem. Concr. Comp. 65 (2016) 83–93.
[24] D. Snoeck, K. Van Tittelboom, S. Steuperaert, P. Dubruel, N. De Belie, Self-healing cementitious materials by the combination of microfibres and superabsorbent polymers, J. Intell. Mater. Syst. Struct. 25 (2014) 13–24.
[25] 225-SAP, Application of Superabsorbent Polymers (SAP) in Concrete Construction, in: V. Mechtcherine, H.W. Reinhardt (Eds.), RILEM State-Of-The-Art Report Prepared by Technical Committee 225-SAP, 2012, p. 165.
[26] C. Schröfl, D. Snoeck, V. Mechtcherine, A review of characterisation methods for superabsorbent polymer (SAP) samples to be used in cement-based construction materials - report of the RILEM TC 260-RSC, Mater. Struct. 50 (2017) 1–19.
[27] O.M. Jensen, P.F. Hansen, Water-entrained cement-based materials I. Principles and theoretical background, Cem. Concr. Res. 31 (2001) 647–654.
[28] O.M. Jensen, P.F. Hansen, Water-entrained cement-based materials II. Experimental observations, Cem. Concr. Res. 32 (2002) 973–978.
[29] D. Snoeck, O.M. Jensen, N. De Belie, The influence of superabsorbent polymers on the autogenous shrinkage properties of cement pastes with supplementary cementitious materials, Cem. Concr. Res. 74 (2015) 59–67.
[30] D. Snoeck, L. Pel, N. De Belie, The water kinetics of superabsorbent polymers during cement hydration and internal curing visualized and studied by NMR, Sci. Rep. 7 (2017) 1–14.
[31] V. Mechtcherine, C. Schröfl, M. Wyrzykowski, M. Gorges, D. Cusson, J. Margeson, N. De Belie, D. Snoeck, K. Ichimiya, S.-I. Igarashi, V. Falikman, S. Friedrich, J. Bokern, P. Kara, P. Lura, A. Marciniak, H.-W. Reinhardt, S. Sippel, A.B. Ribeiro, J. Custódio, G. Ye, H. Dong, J. Weiss, Effect of superabsorbent polymers (SAP) on the freeze-thaw resistance of concrete: results of a RILEM interlaboratory test, Mater. Struct. 50 (2017) 1–19.
[32] S. Mönnig, P. Lura, Superabsorbent polymers - an additive to increase the freeze-thaw resistance of high strength concrete, in: C.U. Grosse (Ed.), Adv Constr Mater, Springer Berlin Heidelberg, Berlin, 2007, pp. 351–358.
[33] V. Mechtcherine, E. Secrieru, C. Schröfl, Effect of superabsorbent polymers (SAPs) on rheological properties of fresh cement-based mortars – development of yield stress and plastic viscosity over time, Cem. Concr. Res. 67 (2015) 52–65.
[34] H.X.D. Lee, H.S. Wong, N.R. Buenfeld, Potential of superabsorbent polymer for self-sealing cracks in concrete, Adv. Appl. Ceram. 109 (2010) 296–302.
[35] H.X.D. Lee, H.S. Wong, N.R. Buenfeld, Self-sealing of cracks in concrete using superabsorbent polymers, Cem. Concr. Res. 79 (2016) 194–208.
[36] D. Snoeck, S. Steuperaert, K. Van Tittelboom, P. Dubruel, N. De Belie, Visualization of water penetration in cementitious materials with superabsorbent polymers by means of neutron radiography, Cem. Concr. Res. 42 (2012) 1113–1121.
[37] D. Snoeck, Self-healing and microstructure of cementitious materials with microfibres and superabsorbent polymers, Struct Eng, Ghent University, Ghent, 2015, p. 364.
[38] M. Kanematsu, I. Maruyama, T. Noguchi, H. Iikura, N. Tsuchiya, Quantification of water penetration into concrete through cracks by neutron radiography, Nucl. Instrum. Methods Phys. Res. Sect. A 605 (2009) 154–158.
[39] V. Cnudde, M. Dierick, J. Vlassenbroeck, B. Masschaele, E. Lehmann, P. Jacobs, L.V. Hoorebeke, High-speed neutron radiography for monitoring the water absorption by capillarity in porous materials, Nucl. Instrum. Methods Phys. Res., Sect. B 266 (2008) 155–163.
[40] K. Van Tittelboom, D. Snoeck, P. Vontobel, F.H. Wittmann, N. De Belie, Use of neutron radiography and tomography to visualize the autonomous crack sealing efficiency in cementitious materials, Mater. Struct. 46 (1–2) (2012) 105–121.
[41] C. Schröfl, V. Mechtcherine, A. Kaestner, P. Vontobel, J. Hovind, E. Lehmann, Transport of water through strain-hardening cement-based composite (SHCC) applied on top of cracked reinforced concrete slabs with and without hydrophobization of cracks - investigation by neutron radiography, Constr. Build. Mater. 76 (2015) 70–86.
[42] P. Zhang, F.H. Wittmann, T.J. Zhao, E. Lehmann, Neutron imaging of water penetration into cracked steel reinforced concrete, Phys. B 405 (2010) 1866–1871.
[43] P. Zhang, F.H. Wittmann, T.J. Zhao, E. Lehmann, L. Tian, P. Vontobel, Observation and quantification of water penetration into strain hardening cement-based composites (SHCC) with multiple cracks by means of neutron radiography, Nucl. Instrum. Methods A 620 (2010) 414–420.
[44] C. Schröfl, V. Mechtcherine, P. Vontobel, J. Hovind, E. Lehmann, Sorption kinetics of superabsorbent polymers (SAPs) in fresh Portland cement-based pastes visualized and quantified by neutron radiography and correlated to the progress of cement hydration, Cem. Concr. Res. 75 (2015) 1–13.
[45] P. Trtik, B. Muench, W.J. Weiss, G. Herth, A. Kaestner, E. Lehmann, P. Lura, Neutron tomography measurements of water release from superabsorbent polymers in cement Paste, in: W. Brameshuber (Ed.), International RILEM Conference on Material Science, RILEM Publications S.A.R.L., Aachen, 2010, pp. 175–185.
[46] J. Justs, M. Wyrzykowski, D. Bajare, P. Lura, Internal curing by superabsorbent polymers in ultra-high performance concrete, Cem. Concr. Res. 76 (2015) 82–90.
[47] P. Van den Heede, B. Van Belleghem, N.M. Alderete, K. Van Tittelboom, N. De Belie, Neutron radiography based visualization and profiling of water uptake in (un) cracked and autonomously healed cementitious materials, Materials 9 (2016) 1–24.
[48] V.C. Li, Y.M. Lim, Y.W. Chan, Feasibility study of a passive smart self-healing cementitious composite, Compos. B 29 (1988) 819–827.
[49] D. Snoeck, D. Schaubroeck, P. Dubruel, N. De Belie, Effect of high amounts of superabsorbent polymers and additional water on the workability, microstructure and strength of mortars with a water-to-cement ratio of 0.50, Constr. Build. Mater. 72 (2014) 148–157.
[50] D. Snoeck, L.F. Velasco, A. Mignon, S. Van Vlierberghe, P. Dubruel, P. Lodewyckx, N. De Belie, The effects of superabsorbent polymers on the microstructure of cementitious materials studied by means of sorption experiments, Cem. Concr. Res. 77 (2015) 26–35.
[51] E. Lehmann, P. Vontobel, I. Wiezel, Properties of the radiography facility NEUTRA at SINQ and its use as European reference facility, NDT&E Int 16 (2001) 191–202.
[52] R. Hassanein, Correction Methods for the Quantitative Evaluation of Thermal Neutron Tomography, ETH Zurich, Zurich, 2006, p. 149.
[53] Y. Yao, Y. Zhu, Y. Yang, Incorporation of SAP particles as controlling pre-existing flaws to improve the performance of ECC, Constr. Build. Mater. 28 (2011) 139–145.
[54] M.T. Hasholt, O.M. Jensen, K. Kovler, S. Zhutovsky, Can superabsorbent polymers mitigate autogenous shrinkage of internally cured concrete without compromising the strength? Constr. Build. Mater. 31 (2012) 226–230.